13th International Symposium on Turbulence and Shear Flow Phenomena (TSFP13)
Montreal, Canada, June 25–28, 2024

SPECTRAL ANALYSIS OF THE RECOVERY OF THE ENERGY-CONTAINING SCALES OF MOTION IN TURBULENT BOUNDARY LAYERS

Antonio Matas, Kevin Liu, Ezhilsabareesh Kannadasan, Callum Atkinson, Julio Soria
Laboratory for Turbulence Research in Aerospace
Combustion (LTRAC),
Department of Mechanical and Aerospace Engineering
Monash University
Clayton, 3800, Victoria, Australia
antonio.matassalva@monash.edu

ABSTRACT

This study investigates using direct numerical simulation (DNS) the recovery of the energy-containing scales of motion (energy-containing motions) when these are removed at the inflow boundary condition of a flat plate zero-pressure-gradient turbulent boundary layer (ZPG-TBL). Specifically, the removed energy-containing motions are those that act as net energy providers in the turbulent energy cascade, and are thus identified as the velocity fluctuations with wall-normal and spanwise wavelength coordinate associated with an energy-supplying contribution in the spanwise spectra of the interscale turbulent transport. The removal of these motions results in a significant reduction of the Reynolds stresses and in the elimination of net turbulent kinetic energy generation in the buffer layer. With dissipation globally dominating over production, turbulent energy attenuates. However, as the flow progresses downstream, in the buffer layer production from the mean shear intensifies, eventually surpassing dissipation. The excess of turbulent kinetic energy in the buffer layer is transported to lower and upper locations, and the canonical ZPG-TBL state is eventually recovered, with locations closer to the wall recovering more rapidly. Importantly, the recovery of the turbulent motions in the outer-wall is shown to be preceded by an energy flux coming from the buffer layer, suggesting that the near-wall region do not only recovers faster but that it has a role in the recovery of the outer turbulent motions. Analysis of spanwise spectral energy densitiy of the streamwise velocity and of the streamwise vorticity suggests that near-wall streaks are the initial coherent energy-containing motions formed, with quasi-streamwise vortices developing only further downstream.

INTRODUCTION

Wall-bounded turbulence is often conceptualised as a superposition of energy-containing eddying motions spanning a wide range of sizes across the boundary layer. A recurrent approach to study these dominant flow motions has consisted in conducting numerical experiments that simulate isolated length scales in the flow, achieved by considering a reduced subset of the flow and/or specifying a restricted range of wavenumbers (Jiménez & Lozano-Durán (2016)). These experiments provided evidence supporting that energy-containing motions under these simulating conditions complete a self-sustaining regeneration cycle in the near-wall (Jimenez & Moin (1991); Hamilton *et al.* (1995); Jimenez & Pinelli (1999)) and in the logarithmic (Flores & Jiménez (2010); Hwang & Cossu (2011)) and outer regions (Hwang & Cossu (2010)), suggesting the possibility that their generation at each length scale may rely on an autonomous process independent of the rest of the flow. However, despite the body of numerical work quantifying the nature of the energy-containing motions of wall-turbulence, the specific details of how these motions originate remain unclear. In this work, a direct numerical simulation (DNS) of a flat plate zero-pressure-gradient turbulent boundary layer (ZPG-TBL) in which the energy-containing motions are removed at the inflow boundary condition is undertaken to investigate this aspect. Specifically, the energy-containing motions that are removed correspond to those motions providing net energy to the other motions as accounted for in the non-linear term of the Navier-Stokes equations. Ultimately, this experiment aims to unveil the role that different spanwise length scales might play in the formation of the energy-containing motions by examining the role of the spanwise scales involved in recovering these motions when they are removed at an upstream flow cross-plane.

METHOD

In the following, the streamwise, wall-normal, and spanwise spatial directions are denoted by x, y and z, and the corresponding instantaneous velocities by $\widetilde{u}$, $\widetilde{v}$, and $\widetilde{w}$. In index notation, these are indicated by x_i and $\widetilde{u_i}$ with $i = \{1,2,3\}$. The subscript $\cdot|_{x_i}$ is used to express the coordinate value at which a variable is evaluated. The ensemble average $\langle\cdot\rangle$ denotes averaging over the spanwise homogeneous direction and time. Mean values are denoted by capital letters, $U_i = \langle\widetilde{u_i}\rangle$, while fluctuations with respect to these averages by lower-cases, $u_i = \widetilde{u_i} - U_i$. The superscript $+$ denotes viscous units, which are defined appropriately in terms of the kinematic viscosity ν and the streamwise-dependent friction velocity $u_\tau = \sqrt{\tau_w/\rho}$, where $\tau_w = \mu\partial U/\partial y|_{y=0}$ is the mean wall shear stress, μ is the dynamic viscosity and ρ is the constant fluid density. The free-stream velocity is denoted by U_∞ and the 99% boundary layer thickness by δ. The Reynolds number based on the momentum thickness, θ, is defined as $Re_\theta = U_\infty\theta/\nu$.

The turbulent boundary layer flow is directly simulated numerically over a smooth no-slip wall with spanwise periodicity and streamwise non-periodic inflow and outflow. The

TBL-DNS code solves the primitive-variable formulation of the Navier–Stokes equations for incompressible fluids using a fractional step method (Harlow & Welch (1965); Perot (1993)) with x-y staggered three-point compact finite differences (Lele (1992)) for the spatial discretization of the derivatives in the streamwise and wall-normal directions, and second order discretization for the pressure. Fourier decomposition in the periodic spanwise direction is used, dealiased using the $2/3$ rule. The equations are stepped forward in time using a semi-implicit low storage three sub-step Runge-Kutta scheme (Simens *et al.* (2009)). A detailed description of the code can be found in Simens *et al.* (2009) and Sillero *et al.* (2013). The DNS setup of the present simulation consists of two concatenated domains that run synchronously. The first domain, BL_1, runs a reference ZPG-TBL. This domain generates its own inflow by re-scaling the velocity fluctuations of a downstream cross-plane, $x = X_r$, while fixing the inflow mean velocity to a prescribed profile to ensure a constant inflow mass flux (Sillero *et al.* (2013)). BL_2 runs a ZPG-TBL DNS with its inflow obtained by transferring at each time step the velocity cross-plane of BL_1 located at $x = X_t$ such that $Re_{\theta|_{X_t}} = 2500$, with the energy-containing motions filtered out, as detailed below. Convective boundary conditions are applied at the outflow of both domains and the mean pressure gradient is controlled and kept small by imposing a streamwise dependent wall-normal velocity, constant in time, at the upper boundary (Sillero *et al.* (2013)). Parameters for the DNSs performed are presented in table 1.

The energy-containing motions of the turbulence are understood as those fluid motions that carry most of the kinetic energy and which, through a cascading process, supply net energy to the rest of fluid motions. Since in wall-bounded turbulence these motions can be characterised by their spanwise length scales (Flores & Jiménez (2010); Hwang (2015)), the TKE equation for each spanwise Fourier mode provides an effective framework to identify and study these motions. This equation can be derived by Fourier-transforming one-half of the trace of the equation of the two-point correlations of the velocity fluctuations (Lumley (1964); Lee & Moser (2019)) or equivalently, by starting from the Navier–Stokes equations for the Fourier modes of the velocity and pressure fluctuations (Bolotnov *et al.* (2010); Mizuno (2016); Cho *et al.* (2018)). We adapt the formulation in Mizuno (2016) for channel flows to ZPG-TBLs, and express the evolution equation for the TKE spectrum, $\widehat{e} = \widehat{u}_i \widehat{u}_i^*/2$ with $\widehat{\cdot}$ denoting Fourier expansion coefficient in the spanwise direction and $\cdot^*$ complex conjugation, as:

$$\begin{aligned}\frac{\partial \overline{\widehat{e}(x,y,k_z)}}{\partial t} = &\underbrace{\mathrm{Re}\left\{-U_j \frac{\partial \overline{\widehat{e}}}{\partial x_j}\right\}}_{\widehat{C}} + \underbrace{\mathrm{Re}\left\{\overline{-\widehat{u}_i^* \widehat{u}_j} \frac{dU_i}{dx_j}\right\}}_{\widehat{P}} \\ &+ \underbrace{\left(-\nu \overline{\frac{\partial \widehat{u}_i}{\partial x_j}\frac{\partial \widehat{u}_i^*}{\partial x_j}}\right)}_{\widehat{\varepsilon}} + \underbrace{\mathrm{Re}\left\{\overline{-\widehat{u}_i^* \frac{\partial}{\partial x_j}\widehat{(u_i u_j)}}\right\}}_{\widehat{T}_{turb}} \\ &+ \underbrace{\mathrm{Re}\left\{-\frac{1}{\rho}\frac{\partial \overline{\widehat{p}\widehat{v}^*}}{\partial x_j}\right\}}_{\widehat{T}_p} + \underbrace{\nu \frac{\partial^2 \overline{\widehat{e}}}{\partial x_j^2}}_{\widehat{T}_\nu}\end{aligned} \tag{1}$$

with $(\partial/\partial x_1, \partial/\partial x_2, \partial/\partial x_3) = (\partial/\partial x, \partial/\partial y, ik_z)$ and summation implied over repeated indices. The overline $\bar{\cdot}$ indicates time averaging and $\mathrm{Re}\{\cdot\}$ means the real part of the complex number. The left hand side of the equation represents the rate of change of TKE of each spanwise Fourier mode. This term vanishes if the flow is statistically steady. The terms on the right-hand side are known as the rate of: (i) mean convection ($\widehat{C}$) (ii) turbulence production ($\widehat{P}$), (iii) viscous dissipation ($\widehat{\varepsilon}$), (iv) turbulent transport ($\widehat{T}_{turb}$), (v) pressure transport ($\widehat{T}_p$) and (vi) viscous transport ($\widehat{T}_\nu$). Note that the only term in the right hand side involving an interaction between spanwise wavenumbers (or scales) is the non-linear turbulent transport term. This term can be further decomposed into a linear and a non-linear term (Mizuno (2016)):

$$\begin{aligned}\widehat{T}_{turb}(x,y,k_z) = &\underbrace{\mathrm{Re}\left\{-\frac{1}{2}\frac{d}{dy}\overline{\widehat{u}_i^*(\widehat{u_i v})}\right\}}_{\widehat{T}^{\perp}_{turb}} \\ &+ \underbrace{\mathrm{Re}\left\{\frac{\partial}{\partial x_j}\overline{\widehat{u}_i^*(\widehat{u_i u_j})} - \frac{1}{2}\frac{d}{dy}\overline{\widehat{u}_i^*(\widehat{u_i v})}\right\}}_{\widehat{T}^{\parallel}_{turb}}\end{aligned} \tag{2}$$

The first term in the right hand side of equation (2), the linear term, yields the transport of turbulent energy in the wall-normal direction at constant spanwise wavenumber, and therefore is referred to as the *spatial turbulent transport*. The second term in the expression, the non-linear term, yields the turbulent energy transport between spanwise wavenumbers at constant y, and is referred to as the *interscale turbulent transport*. Note that this term accounts for the redistribution of turbulent kinetic energy among the various scales of motion and does not make any contribution to the total energy budget:

$$\sum_k \widehat{T}^{\parallel}_{turb}(x,y,k_z) = 0 \tag{3}$$

It should be noticed that the decomposition of the turbulent transport term is not unique. The adopted decomposition follows Mizuno (2016) and has also been adopted in other studies in the literature (Lee & Moser (2019)).

It is reasonable to argue that the bulk of the energy-containing motions would leave a distinct imprint on the energy spectrum of $\hat{T}^{\parallel}_{turb}$, in the form of a discernible region of negative energy - where a negative value in the spectrum indicates a net energy-supplying contribution. That is, that region would be mostly representative of the scales of motion that are net energy providers to the other motions. Figure 1 presents the premultiplied spectral energy density of $\hat{T}^{\parallel}_{turb}$ at the transfer plane. A contour enclosing the region characterised by negative values in the spectrum has been approximated and is represented in the figure by the solid black curve. The inflow boundary condition of BL_2 is generated by transferring at each time-step the velocity field at the transfer plane to the inlet of BL_2 with the energy-containing motions removed. This filtering is accomplished by setting to zero the velocity fluctuations with coordinate (y, λ_z) located within the approximated contour. Since the DNS code employed is spectral in the spanwise direction, this filtering operation is easily implemented. Note that this filtering operation does not modify the zeroth spanwise Fourier mode and consequently, *i.e.,* preserves the mean mass flow rate.

Finally, note that the budget equation of TKE, $e = \langle u_i u_i \rangle/2$, is obtained by summing each term of equation 1 over

Table 1. Parameters of the turbulent boundary layer. Along the three axes, L_x, L_y and L_z are the domain dimensions and N_x,N_y and N_z are the collocation grid sizes. T is the total time over which statistics have been accumulated after transients. δ and u_τ taken at the at the BL_1 transfer plane, X_t.

Case	Re_θ	$(L_x, L_y, L_z)/\delta$	Δx^+, $\Delta y^+_{\min}$, Δz^+	N_x, N_y, N_z	Tu_τ/δ
BL_1	$290-4000$	$101.64, 4.82, 5.4\pi$	$11, 0.28, 5.51$	$8193, 315, 2730$	8.9
BL_2	$2500-3750$	$48.38, 4.82, 5.4\pi$	$11, 0.28, 5.51$	$3900, 315, 2730$	8.9

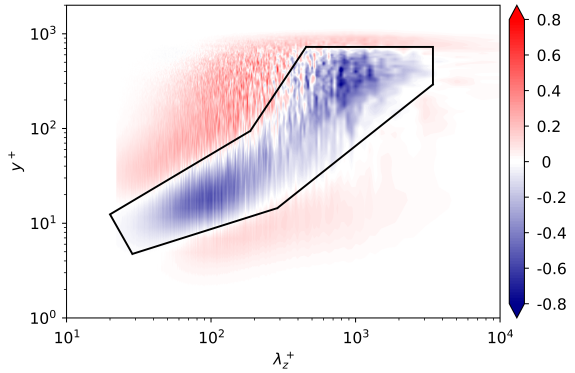

Figure 1. $yk_z\widehat{T}^{\parallel}_{turb}(y,\lambda_z)$ at $x = X_t$. Contour levels are -0.8(0.1)0.8 times the absolute maximum in the spectrum.

all wavenumbers:

$$\frac{\partial e(x,y)}{\partial t} = C + P + \varepsilon + T_{turb} + T_p + T_\nu \tag{4}$$

The balance between production and dissipation yields the source term of TKE, $\xi = P + \varepsilon$. This term categorizes wall-normal locations as either an energy-source ($\xi > 0$), energy-sink ($\xi < 0$) or energy-neutral ($\xi = 0$). Finally, note that the sum of the various transport terms which describes how energy is redistributed among different wall-normal locations corresponds to the divergence of an energy flux, $\phi = \int_0^y (T_{turb} + T_p + T_\nu)dy$, that connects energy-source and energy-sink regions.

RESULT

The effect of removing the energy-containing motions at the inflow boundary condition of a ZPG-TBL is first studied by examining the evolution of the profiles of the mean velocity and Reynolds stresses. The profiles of the single-point TKE budget terms are then discussed. Finally, the spanwise spectral energy density of the streamwise velocity and of the streamwise vorticity are examined.

The profiles of the mean velocity, the root-mean-squared (rms) turbulent velocity fluctuations and the Reynolds shear stress of BL_2 are presented and compared to those of BL_1 in figure 2. The streamwise coordinate $\tilde{x}$, common to both BLs, defines the streamwise location at which quantities are being evaluated based on the distance from this streamwise location to the transfer plane when referring to BL_1 and to the domain's inlet when referring to BL_2. This distance is expressed in terms of the boundary layer thickness measured at the transfer plane, $\delta_{|_{X_t}}$. The streamwise locations shown in the figure were chosen by examining the evolution of the absolute and relative differences of the mean and fluctuating velocities at fixed y^+ between BL_1 and BL_2 (not shown), and selecting the streamwise locations which best represent the overall evolution of these quantities. The removal of the energy-containing motions at the inlet of BL_2 results, as expected, in a significant decrease in the (ensemble averaged) rms of turbulent velocity fluctuations and Reynolds shear stress. Since the filtering operation does not affect the zeroth spanwise Fourier mode, the mean velocity profile of BL_2 is identical to that of BL_1, *i.e.,* the mean flow rate is preserved. The mean velocity profile at $\tilde{x} = 0.5\delta_{|_{X_t}}$, when compared to $\tilde{x} = 0\delta_{|_{X_t}}$, has amplified above the viscous sublayer, where the profile scales linearly with distance from the wall. This amplification of the profile, overall by a constant factor, indicates a lower value of the friction velocity at the downstream location. Indeed, as the flow progresses downstream from the inlet of BL_2, the mean velocity profile has to adjust to the (remaining) Reynolds shear stress. This adjustment results in a reduction of the wall shear stress, $\tau_w = \mu \partial U/\partial y_{|_{y=0}}$, and thus of the friction velocity, $u_\tau = \sqrt{\tau_w/\rho}$.

Note that the streamwise velocity fluctuations are, on average, the only ones that receive energy directly from the mean flow through the production term. Part of this energy is then redistributed to the other two velocity components by action of the pressure. When comparing the mean velocity profile at $\tilde{x} = 0.5\delta_{|_{X_t}}$ and $\tilde{x} = 1.75$, despite a reduction in the friction velocity that results in an amplified profile at $\tilde{x} = 1.75$, the profiles in the buffer layer at both streamwise locations align closely over a certain wall-normal range. This implies that mean kinetic energy is lost to streamwise turbulent energy at these wall-normal locations, consistent with the evolution of a buffer layer peak in the rms of the streamwise velocity fluctuations. With the strengthening of the streamwise velocity fluctuations in the buffer layer, the recovery of the transversal, *i.e.,* wall-normal and spanwise, velocity components follows at the downstream locations. The evolution of the mean velocity profile from $\tilde{x} = 1.75\delta_{|_{X_t}}$ to $\tilde{x} = 6\delta_{|_{X_t}}$ suggests that the friction velocity is gradually recovering to that of BL_1. At $\tilde{x} = 6\delta_{|_{X_t}}$, the profiles of BL_2 in the near-wall overall resemble those of BL_1, while discrepancies are still pronounced in the outer-wall. Comparing the mean velocity and the rms of the streamwise velocity at $\tilde{x} = 6\delta_{|_{X_t}}$ and $\tilde{x} = 20\delta_{|_{X_t}}$, a transfer of mean kinetic energy to the streamwise velocity fluctuations is evident, and it is followed by a recovery in the transversal velocity fluctuations at the downstream locations. Turbulence in the flow therefore recovers and evolves towards the canonical ZPG-TBL state as the flow progresses downstream. Note that most of the streamwise evolution of the profiles is captured within the first $20\delta_{X_t}$, which is followed by a slower recovery that continues until the end of the domain. Hence, it is reasonable to expect that the streamwise extent of BL_2 is large enough to capture the relevant processes that lead the recovery of the energy-containing motions within this domain. The evolution of these profiles shows that the near-wall region recovers faster than the outer region, consistent with the shorter time-scales of the turbulence near the wall. However, whilst the current research suggests that the energy-containing motions in the outer region might exhibit self-sustaining dynamics (Flores &

Jiménez (2010); Hwang & Cossu (2011, 2010)), it remains unclear whether the dynamics in both layers evolve towards the canonical ZPG-TBL state independently or if the faster recovery near the wall influences the recovery in the outer region.

To that end, figure 3 compares the streamwise evolution of the profiles of the terms in the TKE budget equation for BL_1 and BL_2. For BL_1 (figure 3(a)), as is already known for canonical ZPG-TBLs, the viscous sublayer serves as the main energy-sink, while the buffer layer acts as the main energy-source. Note that the excess of TKE produced in the buffer layer is transported towards the lower and upper locations, where energy is finally dissipated. In particular, the sum of all transport terms exhibits its global minimum at the location where the energy-source is most intense, $y^+ \approx 15$, which implies that the energy flux bifurcates at this wall-normal location into a downward and an upper flux. The downward energy flux is shown to be dominated by viscous transport while the upper energy flux by turbulent transport. The logarithmic and outer layers exhibit near energy-neutral conditions, with dissipation slightly exceeding production. It should be pointed that although work in the literature suggests the existence of an energy-source in the outer-layer (Cimarelli *et al.* (2015); Sillero *et al.* (2013)), this source is not observed in our current data. This might suggests that the role and dynamics of the outer region might not be accurately captured. Specifically, the residual of the TKE budget terms exhibits, in viscous units, a maximum of 0.1% within the outer region, at a location which coincides with the reported location of the outer energy-source (Cimarelli *et al.* (2015)). Although this discrepancy exempts from quantifying the influence of the recovery of the inner-wall on the outer motions, it will be argued that it does not prevent from examining whether the more rapidly recovering buffer layer has an influence on the recovery of the outer turbulent motions.

At $\tilde{x} = 0\delta_{|_{X_t}}$ of BL_2 (figure 3(a)), the residual in the TKE budget quantifies the suppression of TKE associated with the removed energy-containing motions. Note that this is the only streamwise location in the domain where, due to the artificial removal of TKE, the residual deviates from zero.The production term has been largely removed, as anticipated by the profile of the Reynolds shear stress at this streamwise location (figure 2(m)). Dissipation, although attenuated, globally dominates over production. At $\tilde{x} = 0.1\delta_{|_{X_t}}$, dissipation remains dominant but has largely attenuated, consistent with the smaller magnitude of the turbulent intensities and of their spatial gradients. The only active transport term is viscous diffusion, which transports (remaining) energy from the buffer layer towards the wall. With the absence of an energy-source, the flow would eventually laminarise. However, at $\tilde{x} = 0.5\delta_{|_{X_t}}$, a weak energy-source within the buffer layer is observed, consistent with the evolution of a peak in the profile of the rms of the streamwise velocity fluctuations (figure 2(a)). Thus, despite turbulent energy attenuating as the flow evolves from the inlet of BL_2, energy from the mean flow continues to be redistributed to the streamwise velocity fluctuations, eventually surpassing the rate of energy dissipation. As the flow advances to $\tilde{x} = 1.75$, the energy-source intensifies in the buffer layer, and an upper energy flux due to turbulent transport supplies energy to the logarithmic layer. Note that while at $\tilde{x} = 1.75\delta_{|_{X_t}}$ an upward energy flux from the buffer layer provides energy to the locations above, turbulent intensities decrease for around $y^+ \gtrsim 150$ from $\tilde{x} = 1.75\delta_{|_{X_t}}$ to $\tilde{x} = 6\delta_{|_{X_t}}$, indicating that turbulence in the outer region is attenuating rather than recovering towards its energy neutral conditions, which would also precede the re-establishment of a potential outer energy-source. Considering the smaller shear and smaller value of the outer energy-source compared to the energy-source in the buffer layer (Cimarelli *et al.* (2015)), it is unlikely that the presented picture would change much despite the current underprediction of the source term in the outer region. That is, even if an outer energy-source were detected and removed by the filtering operation, the upward energy flux from the more rapidly recovering buffer layer would supply energy to the outer region prior to the recovery of the outer energy-source. This implies that the near-wall has a role in, at least accelerating, the recovery of the outer turbulent motions.

Insight into the energy-containing motions that first appear in the flow can be gained by examining the spanwise spectra of the streamwise velocity and streamwise vorticity, presented in Figures 4 and 5, respectively. Note that spectra are premultiplied by k_z to express energy density per $\log k$ on the log-scale plots. Figure 4(a) shows that the removal of the energy-containing motions at the inflow of BL_2 results in the removal of most of the energy in the $k_z E_{uu}$ spectrum, and in particular in the removal of the the near-wall spectral peak, located for BL_1 at $\lambda_z^+ \approx 100$ and $y^+ \approx 15$. This near-wall peak in the $k_z E_{uu}$ spectrum is attributed to the near-wall cycle of streaks of streamwise velocity and quasi-streamwise vortices, and its location is known to be roughly independent of the Reynolds number (Jiménez (2013)). As the flow progresses from the inflow to $x = 6\delta_{|_{X_t}}$, the energy in the $k_z E_{uu}$ spectrum of BL_2 builds around a peak located in the buffer layer, that gradually shifts its location as the flow evolves, while it reduces in the rest of the spectrum. Downstream of $x = 6\delta_{|_{X_t}}$, the spectral energy in $k_z E_{uu}$ gradually propagates towards regions located further away from the wall and into larger spanwise wavelengths. At $x = 0\delta_{|_{X_t}}$, the $k_z E_{\omega_x\omega_x}$ spectrum of BL_1 exhibits two peaks. The peak within the buffer layer is attributed to streamwise vortices, while the peak closer to the wall arises due to vortices created by the no-slip condition at the wall (Jeong *et al.* (1997)). In the spectrum of BL_2, both of these peaks have been removed by the filtering operation that removes the energy-containing motions, and only traces of energy of the streamwise vorticity are detected. No noticeable energy in the spectrum of BL_2 seem to be present for locations $x = 0.5 - 1.75\delta_{|_{X_t}}$. It should be noted that at $x = 1.75\delta_{|_{X_t}}$, the $k_z E_{uu}$ spectrum of BL_2 shows the presence of a peak in the near-wall. This presence of a near-wall peak in the $k_z E_{uu}$ spectrum and the absence of energy in the near-wall of the spectrum of $k_z E_{\omega_x\omega_x}$, suggests the presence of near-wall streaks and the absence of near-wall quasi-streamwise vortices. At $x = 6\delta_{|_{X_t}}$, the $k_z E_{\omega_x\omega_x}$ spectrum of BL_2 exhibits energy peaks at the same locations as those detected in the spectrum of BL_1. In particular, the buffer layer peak in the spectrum suggests the presence of the quasi-streamwise vortices that are involved in the near-wall cycle. This would imply that a near-wall cycle was initiated between $x = 1.75\delta_{|_{X_t}}$ and $x = 6\delta_{|_{X_t}}$.

DISCUSSION

This study has investigated the recovery of the energy-containing motions when they are removed at the inflow boundary condition of a flat plate ZPG-TBL DNS. The bulk of the energy-containing motions has been identified with a distinctive connected (y, λ_z)-region within the spanwise spectral energy density of the interscale turbulent transport with negative value, *i.e.,* a net energy-supplying contribution. The removal of these motions at the inflow boundary condition results in a significant reduction of the Reynolds stresses at this streamwise location. In particular, analysis of the single-point

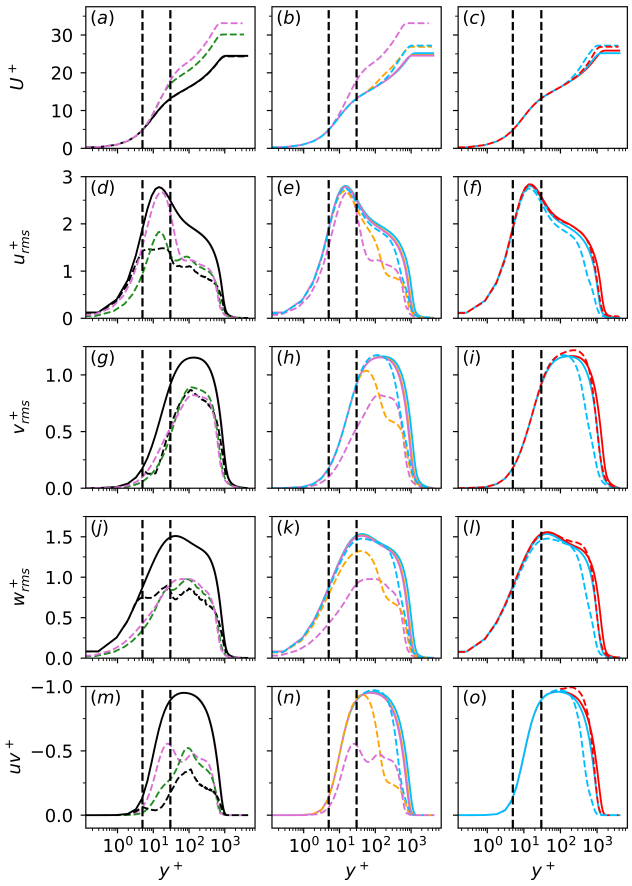

Figure 2. Statistical velocity profiles. (*a-c*) Mean velocity profile. Root-mean-squared of the: (*d-f*) streamwise, (*g-i*) wall-normal (*j-l*) and spanwise velocity fluctuations. (*m-o*) Reynolds shear stress. BL1 (—); BL2 (−−);. Streamwise locations $\tilde{x}/\delta_{X_i}$: 0 (—); 0.5 (—); 1.75 (—); 6 (—); 20 (—); 46 (—);. Vertical dashed black lines are $y^+ = 5$ and $y^+ = 30$.

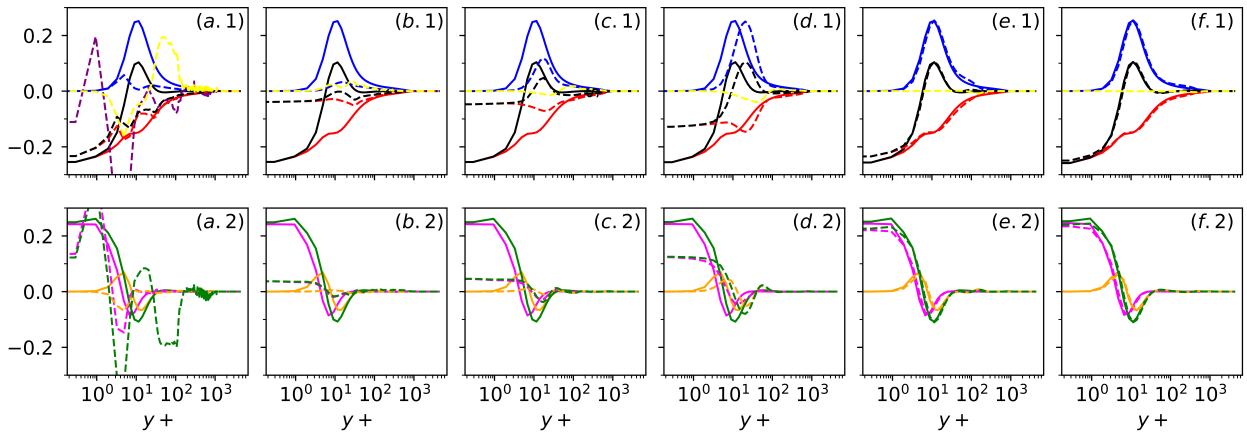

Figure 3. Terms in the TKE budget equation. BL1 (—); BL2 (−−);. Streamwise locations $\tilde{x}/\delta_{X_i}$: (*a*) 0; (*b*) 0.1; (*c*) 0.5; (*d*) 1.75; (*f*) 6; (*g*) 20;. $\partial e^+/\partial t$ (—); P^+ (—); ε^+ (—); ξ^+ (—); C^+ (—); T^+_{turb} (—); T^+_v (—); $\left(T^+_{turb} + T^+_v + T^+_p\right)$ (—);. C in BL_1 and T_p in both BL_1 and BL_2 are small and not shown for better clarity. Similarly, the residual is only plotted at $\tilde{x}/\delta_{X_i} = 0$ of BL_2.

TKE budget terms shows that the turbulent energy-source in the buffer layer is removed, resulting in dissipation globally dominating over the nearly nonexistent production. As the flow progresses downstream, turbulence attenuates due to the prevailing dominance of dissipation. Nonetheless, the production term does not completely decay and eventually surpasses the rate of dissipation in the buffer layer, leading to net energy generation in the streamwise velocity component. With part of this energy redistributed to the other two velocity components, Reynolds shear stress is generated and the energy-source in the buffer layer gradually recovers its intensity. The excess of turbulent kinetic energy in the buffer layer is transported to the lower and upper locations, leading to the eventual recovery of the canonical ZPG-TBL state. The canonical ZPG-TBL state is shown to recover more rapidly in the near-wall region than in the outer region. The lack of an outer energy-source in our data prevented from quantifying the influence of the near-wall on the recovery of the outer-wall. However, it

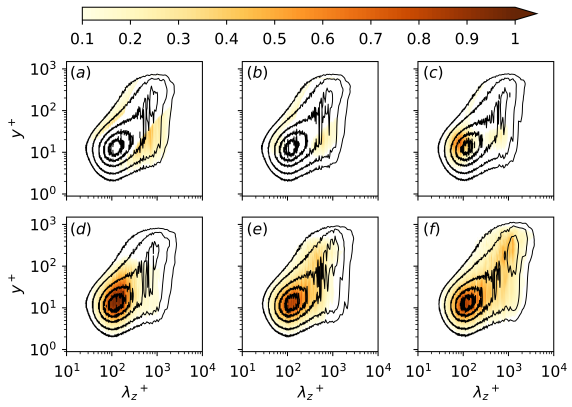

Figure 4. $k_z E_{uu}(\lambda_z, y)$ at streamwise locations $\tilde{x}/\delta_{X_t}$: (a) 0, (b) 0.5, (c) 1.75, (d) 6, (e) 20 and (f) 46. The spectrum of BL_1 is illustrated by the black contour lines, which are $(0.1, 0.2, 0.4, 0.6, 0.8)$ times the maximum of the spectrum at the given location. The colormap visualizes the spectrum of BL_2, with contour levels 0.1 to 1 times the maximum of the spectrum of BL_1 at the transfer plane X_t

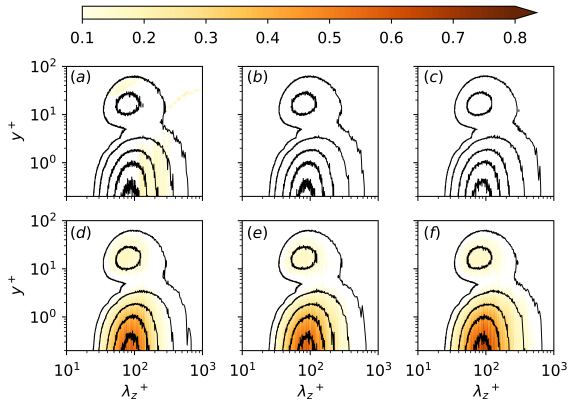

Figure 5. $k_z E_{\omega_x \omega_x}(\lambda_z, y)$ at streamwise locations $\tilde{x}/\delta_{X_t}$: (a) 0, (b) 0.5, (c) 1.75, (d) 6, (e) 20 and (f) 46. The spectrum of BL_1 is illustrated by the black contour lines, which are $(0.1, 0.2, 0.4, 0.6, 0.8)$ times the maximum of the spectrum at the given location. The colormap visualizes the spectrum of BL_2, with contour levels 0.1 to 1 times the maximum of the spectrum of BL_1 at the transfer plane X_t

was argued that even if an outer energy-source were detected and removed by the filtering operation, an energy flux from the more rapidly recovering buffer layer would precede the recovery of the outer energy-source, implying that the near-wall has a role in, at least accelerating, the resurgence of the outer turbulent motions. Analysis of the spanwise spectral energy densitiy of the streamwise velocity and streamwise vorticity suggests that near-wall streaks are the initial coherent energy-containing motions formed with quasi-streamwise vortices only developing further downstream.

ACKNOWLEDGMENT

The support of the Australian Research Council (ARC) and the computational resources provided through NCMAS by the Australian National Computational Infrastructure and the Pawsey Supercomputing Centre for this work are gratefully acknowledged. This work was supported in part by the European Research Council under the CausT grant ERC-ADG-101018287.

REFERENCES

Bolotnov, I., Lahey, R., Drew, D., Jansen, K. & Oberai, A. 2010 Spectral analysis of turbulence based on the dns of a channel flow. *Computers Fluids* **39**, 640–655.

Cho, M., Hwang, Y. & Choi, H. 2018 Scale interactions and spectral energy transfer in turbulent channel flow. *Journal of Fluid Mechanics* **854**, 474–504.

Cimarelli, A., De Angelis, E., Schlatter, P., Brethouwer, G., Talamelli, A. & Casciola, C. 2015 Sources and fluxes of scale energy in the overlap layer of wall turbulence. *Journal of Fluid Mechanics* **771**, 407–423.

Flores, O. & Jiménez, J. 2010 Hierarchy of minimal flow units in the logarithmic layer. *Physics of Fluids* **22**.

Hamilton, J.M., Kim, J. & Waleffe, F. 1995 Regeneration mechanisms of near-wall turbulence structures. *Journal of Fluid Mechanics* **287**, 317–348.

Harlow, F. H. & Welch, J. E. 1965 Numerical calculation of time-dependent viscous incompressible flow of fluid with free surface. *Physics of Fluids* **8** (12), 2182–2189.

Hwang, Y. 2015 Statistical structure of self-sustaining attached eddies in turbulent channel flow. *Journal of Fluid Mechanics* **767**, 254–289.

Hwang, Y. & Cossu, C. 2010 Self-sustained process at large scales in turbulent channel flow. *Physical Review Letters* **105**, 044505.

Hwang, Y. & Cossu, C. 2011 Self-sustained processes in the logarithmic layer of turbulent channel flows. *Physics of Fluids* **23**.

Jeong, J., Hussain, F., Schoppa, W. & Kim, J. 1997 Coherent structures near the wall in a turbulent channel flow. *Journal of Fluid Mechanics* **332**, 185–214.

Jiménez, J. & Lozano-Durán, A. 2016 Coherent structures in wall-bounded turbulence. In *Progress in Wall Turbulence 2*, pp. 37–46. Springer International Publishing.

Jimenez, J. & Moin, P. 1991 The minimal flow unit in near-wall turbulence. *Journal of Fluid Mechanics* **225**, 213–240.

Jimenez, J. & Pinelli, A. 1999 The autonomous cycle of near-wall turbulence. *Journal of Fluid Mechanics* **389**, 335–359.

Jiménez, J. 2013 Near-wall turbulence. *Physics of Fluids* **25**, 1302–.

Lee, M. & Moser, R. D. 2019 Spectral analysis of the budget equation in turbulent channel flows at high reynolds number. *Journal of Fluid Mechanics* **860**, 886–938.

Lele, S. K. 1992 Compact finite difference schemes with spectral-like resolution. *Journal of Computational Physics* **103** (1), 16–42.

Lumley, J. L. 1964 Spectral Energy Budget in Wall Turbulence. *Physics of Fluids* **7** (2), 190–196.

Mizuno, Y 2016 Spectra of energy transport in turbulent channel flows for moderate reynolds numbers. *Journal of Fluid Mechanics* **805**, 171–187.

Perot, J. B. 1993 An analysis of the fractional step method. *Journal of Computational Physics* **108** (1), 51–58.

Sillero, J. A., Jiménez, J. & Moser, R. D. 2013 One-point statistics for turbulent wall-bounded flows at Reynolds numbers up to $\delta^+ \approx 2000$. *Physics of Fluids* **25**, 105–102.

Simens, M. P., Jiménez, J., Hoyas, S. & Mizuno, Y. 2009 A high-resolution code for turbulent boundary layers. *Journal of Computational Physics* **228**, 4128–4231.